Image Segmentation by Image Foresting Transform with Non-smooth Connectivity Functions

Lucy A. C. Mansilla, Paulo A. V. Miranda
Department of Computer Science,
University of São Paulo (USP),
05508-090, São Paulo, SP, Brazil.
Email: lucyacm@vision.ime.usp.br, pmiranda@vision.ime.usp.br

Fábio A.M. Cappabianco
Instituto de Ciência e Tecnologia,
Universidade Federal de São Paulo,
São José dos Campos, SP, Brazil.
Email: cappabianco@unifesp.br

***Abstract*—In the framework of the Image Foresting Transform (IFT), there is a class of connectivity functions that were vaguely explored, which corresponds to the non-smooth connectivity functions (NSCF). These functions are more adaptive to cope with the problems of field inhomogeneity, which are common in MR images of 3 Tesla. In this work, we investigate the NSCF from the standpoint of theoretical and experimental aspects. We formally classify several non-smooth functions according to a proposed diagram representation. Then, we investigate some theoretical properties for some specific regions of the diagram. Our analysis reveals that many NSCFs are, in fact, the result of a sequence of optimizations, each of them involving a maximal set of elements, in a well-structured way. Our experimental results indicate that substantial improvements can be obtained by NSCFs in the 3D segmentation of MR images of 3 Tesla, when compared to smooth connectivity functions.**

***Keywords*-graph search algorithms; image foresting transform; non-smooth connectivity functions**

I. Introduction

Quantitative analysis of brain structures from magnetic resonance images (MRI) has played an important role in research in neurology and can be very useful in the diagnosis and treatment of diseases related to changes in the anatomy of the human brain [1]. Analysis techniques, however, require a precise definition of the extent of the three-dimensional structures under study. This operation called image segmentation is one of the most fundamental and challenging problems in image processing and computer vision [2]. In medical image analysis, accurate segmentation results commonly require the user intervention because of the presence of structures with ill-defined borders, intensity non-standardness among images, field inhomogeneity, noise, artifacts, partial volume effects, and their interplay [1], [3].

Methods based on the Image Foresting Transform (IFT) [4] have been successfully used in the segmentation of 1.5 Tesla MR datasets [5], [6], [7]. However, inhomogeneity effects are stronger in higher magnetic fields, and it is extremely important to define the optimal solution for these images. In the framework of the IFT, there is a class of connectivity functions that were little explored, which corresponds to the non-smooth connectivity functions (NSCF). These functions are more adaptive to cope with the problems of field inhomogeneity, which are common in MR images of 3 Tesla [8]. Their solutions could also be useful in the handling of natural images with strong variation in brightness/shadow.

Historically, the usage of non-smooth connectivity functions (NSCF) has been avoided, because their optimality, in terms of the paths computed by the IFT, may not be guaranteed according to [4]. Early studies only considered the usage of NSCFs, such as f_{euc} (Eq. 3 with 8-connected adjacency), to compute an approximation of the Euclidean distance (EDT) [9], [10], although some other studies by Herman et al. have suggested some practical advantages of using NSCF in the context of image segmentation [11], [12]. More recently, Strand et al. proposed the *Minimum Barrier Distance* (MBD) [13], which, in digital setting, leads to a non-smooth connectivity function. In empirical comparisons, a favorable outcome has been reported for MBD [13] [1]. Also, in other recent works, it has been proven that some non-smooth connectivity functions can lead to optimum results according to other optimality criteria, such as a graph-cut measure [14], [15], or an energy function for optimum boundary tracking [16]. This brought new lights to the research involving NSCF.

In this work, we investigate the NSCF from the standpoint of theoretical and experimental aspects. We formally classify several non-smooth functions according to a proposed diagram representation. Then, we investigate some theoretical properties for some specific regions of the diagram. Our analysis reveals that many NSCFs are, in fact, the result of a sequence of optimizations, each of them involving a maximal set of elements, in a well-structured way. This process resembles the original definition of *Iterative Relative Fuzzy Connectedness* (IRFC) [17], which was defined as the result of a sequence of optimizations by *Relative Fuzzy Connectedness* (RFC) [18]. Our experimental results, using a robot user [19], indicate that substantial improvements can be obtained by NSCFs in the segmentation of MR images of 3 Tesla, when compared to smooth connectivity functions, and their related methods [17], [20].

For the sake of completeness in presentation, Section II includes the relevant previous work of image segmentation by IFT. Our analysis of non-smooth connectivity functions

[1] In [13], an algorithm that finds an approximation of the *Minimum Barrier Distance* was considered, by computing two IFTs separately, one for each term in Eq. 5.

is presented in Section III. In Section IV, we evaluate the NSCFs in the segmentation of MR images of 3 Tesla, and our conclusions are stated in Section V.

II. Image Foresting Transform

An image can be interpreted as a graph $G = (\mathcal{I}, \mathcal{A})$ whose nodes are the image pixels in its image domain $\mathcal{I} \subset Z^N$, and whose arcs are the pixel pairs (s,t) in $\mathcal{A}$ (e.g., 4-neighborhood, or 8-neighborhood, in case of 2D images, and 6-neighbors in 3D). The *adjacency relation* $\mathcal{A}$ is a binary relation on $\mathcal{I}$. We use $t \in \mathcal{A}(s)$ and $(s,t) \in \mathcal{A}$ to indicate that t is adjacent to s. Each arc $(s,t) \in \mathcal{A}$ may have a weight $w(s,t) \geq 0$, such as a dissimilarity measure between pixels s and t (e.g., $w(s,t) = |I(t) - I(s)|$ for a single channel image with values given by $I(t)$).

For a given image graph $G = (\mathcal{I}, \mathcal{A})$, a path $\pi_t = \langle t_1, t_2, \ldots, t_n = t \rangle$ is a sequence of adjacent pixels with terminus at a pixel t. A path is *trivial* when $\pi_t = \langle t \rangle$. A path $\pi_t = \pi_s \cdot \langle s,t \rangle$ indicates the extension of a path π_s by an arc (s,t). A *predecessor map* is a function P that assigns to each pixel t in $\mathcal{I}$ either some other adjacent pixel in $\mathcal{I}$, or a distinctive marker nil not in $\mathcal{I}$ — in which case t is said to be a *root* of the map. A *spanning forest* is a predecessor map which contains no cycles — i.e., one which takes every pixel to nil in a finite number of iterations. For any pixel $t \in \mathcal{I}$, a spanning forest P defines an induced path π_t^P recursively as $\langle t \rangle$ if $P(t) = nil$, and $\pi_s^P \cdot \langle s,t \rangle$ if $P(t) = s \neq nil$.

A *connectivity function* computes a value $f(\pi_t)$ for any path π_t, usually based on arc weights. A path π_t is *optimum* if $f(\pi_t) \leq f(\tau_t)$ for any other path τ_t in G. By taking to each pixel $t \in \mathcal{I}$ one optimum path with terminus t, we obtain the optimum-path value $V(t)$, which is uniquely defined by $V(t) = \min_{\forall \pi_t \text{ in } G}\{f(\pi_t)\}$. The *image foresting transform* (IFT) [4] takes an image graph $G = (\mathcal{I}, \mathcal{A})$, and a path-value function f; and assigns one optimum path π_t to every pixel $t \in \mathcal{I}$ such that an *optimum-path forest* P is obtained — i.e., a spanning forest where all induced paths are optimum. However, f must be *smooth* (Definition 1), otherwise, the paths may not be optimum, as demonstrated in [4].

Definition 1 (Smooth path-value function)**.** *A path-value function f is* smooth *if for any node $t \in \mathcal{I}$, there is a simple optimum path π_t (no repeated vertices), which either is trivial, or has the form $\pi_s \cdot \langle s,t \rangle$ where*

(C1) $f(\pi_s) \leq f(\pi_t)$,

(C2) π_s *is optimum,*

(C3) π_s *is optimum, and for any optimum path π'_s, $f(\pi'_s \cdot \langle s,t \rangle) = f(\pi_t)$* [2].

Any path π_t^P encoded in an optimum-path forest P (i.e., the paths starting in a root node) is a complete-optimum path, according to the following definition:

Definition 2 (Complete-optimum path)**.** *A path $\pi_{t_n} = \langle t_1, t_2, \ldots, t_n \rangle$ is* complete optimum *if all paths $\pi_{t_i} = \langle t_1, t_2, \ldots, t_i \rangle$, $i = 1, 2, \ldots, n$ are optimum paths.*

[2]Our condition C3 corresponds, in fact, to the intersection of the original conditions C2 and C3 from [4], in order to keep the diagram easier.

The cost of a trivial path $\pi_t = \langle t \rangle$ is usually given by a handicap value $H(t)$, while the connectivity functions for non-trivial paths follow a path-extension rule. For example:

$$f_{\max}(\pi_s \cdot \langle s,t \rangle) = \max\{f_{\max}(\pi_s), w(s,t)\} \quad (1)$$

$$f_{\Sigma}(\pi_s \cdot \langle s,t \rangle) = f_{\Sigma}(\pi_s) + w(s,t) \quad (2)$$

$$f_{euc}(\pi_s \cdot \langle s,t \rangle) = \|t - R(\pi_s)\|^2 \quad (3)$$

where $w(s,t) \geq 0$ is a fixed arc weight, and $R(\pi_t)$ is the origin/root of a path π_t. The function f_{euc} may not be smooth, depending on the adjacency $\mathcal{A}$ [4].

We consider image segmentation from two seed sets, $\mathcal{S}_o$ and $\mathcal{S}_b$ ($\mathcal{S}_o \cap \mathcal{S}_b = \emptyset$), containing pixels selected inside and outside the object, respectively. The search for optimum paths is constrained to start in $\mathcal{S} = \mathcal{S}_o \cup \mathcal{S}_b$ (i.e., $H(t) = 0$ for all $t \in S$, and $H(t) = +\infty$ otherwise). The image is partitioned into two optimum-path forests — one rooted at the internal seeds, defining the object, and the other rooted at the external seeds, representing the background [21]. A label, $L(t) = 1$ for all $t \in \mathcal{S}_o$ and $L(t) = 0$ for all $t \in \mathcal{S}_b$, is propagated to all unlabeled pixels during the computation [4].

A. General IFT Algorithm

Algorithm 1 obtains an optimum-path forest P by minimizing a smooth path-value function f, or a spanning forest P in the case of a non-smooth function.

Algorithm 1. – General IFT Algorithm

Input:	Image graph $(\mathcal{I}, \mathcal{A})$, seed sets $\mathcal{S}_o$ and $\mathcal{S}_b$, and path-value function f.
Output:	Optimum-path forest P, the minimum path-value map V and label map L.
Auxiliary:	Priority queue Q, variable tmp, and an array of $status$.

```
1.  For each t ∈ S_o, do L(t) ← 1.
2.  For each t ∈ S_b, do L(t) ← 0.
3.  For each t ∈ I, do
4.      Set P(t) ← nil and V(t) ← f(⟨t⟩).
5.      Set status(t) ← 0.
6.      If V(t) ≠ +∞, then insert t in Q.
7.  While Q ≠ ∅, do
8.      Remove s from Q such that V(s) is minimum.
9.      Set status(s) ← 1.
10.     For each t ∈ A(s), such that status(t) = 0, do
11.         Compute tmp ← f(π_s^P · ⟨s,t⟩).
12.         If tmp < V(t), then
13.             If V(t) ≠ +∞, then remove t from Q.
14.             Set P(t) ← s, V(t) ← tmp.
15.             L(t) ← L(s) and insert t in Q.
```

The "for" loops initialize maps and insert pixels with finite trivial-path values in Q (Lines 1–6). The minima of the initial map V compete with each other and some of them become roots of the forest. The main loop computes optimum paths from the minima to every pixel s in a non-decreasing order of value (Lines 7–15). At each iteration, a path π_s^P of minimum value $V(s)$ is obtained in P when we remove its last pixel s from Q (Line 8). The rest of the lines evaluate if the path

$\pi_s^P \cdot \langle s,t \rangle$ that reaches an adjacent pixel t through s is cheaper than the current path π_t^P in P and update Q, $V(t)$, $L(t)$, and $P(t)$ accordingly.

III. Non-smooth connectivity functions

Clearly, from Definition 1, we have that a connectivity function is not smooth if it doesn't satisfy at least one of the conditions C1, C2 or C3. Note that, if a function f does not satisfy C2, this implies that the condition C3 is not satisfied either. In order to further distinguish between different classes of non-smooth functions, we also evaluate the functions with respect to the condition C4, which is defined below:

Definition 3 (Condition C4)**.** *A path-value function f satisfies the condition C4, if for any node $s \in \mathcal{I}$ the following condition is verified $\forall t \in \mathcal{A}(s)$:*

- *For any paths π_s and π'_s ending at s, if $f(\pi_s) = f(\pi'_s)$, then we have $f(\pi_s \cdot \langle s,t \rangle) = f(\pi'_s \cdot \langle s,t \rangle)$.*

For a general image graph, the classification of various non-smooth functions into the sets C1, C2, C3, and C4 (such that a function f is in a set C_i if and only if it satisfies the condition C_i) is shown in the proposed diagram illustrated in Figure 1. The functions $f^{bkg}_{\max}$, f_ω, $f^{\circlearrowleft}_\omega$, $f_{i,\omega}$, and $f_{o,\omega}$ were studied in [16], [14], [15] [3]. The other functions (i.e., $f_{\Sigma\max}$, $f_\updownarrow$, $f_{\max|\triangle I|}$, $f_{\Sigma|\triangle I|}$, f_I, and $f^{lex}_{\Sigma\max}$) are defined in the Appendix section, including a proof of their respective positions in the proposed diagram.

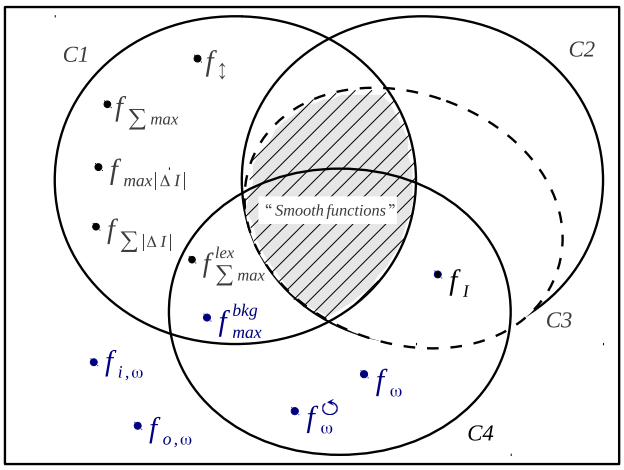

Fig. 1. Schematic representation of the relations between smooth and non-smooth connectivity functions: C1, C2, C3, and C4 are sets of connectivity functions that satisfy these respective conditions for a general graph.

The next propositions reveal some interesting theoretical properties of any non-smooth connectivity function $f \in (C1 \cap C4) \setminus C2$.

Proposition 1. *Consider a connectivity function f, classified as $f \in (C1 \cap C4) \setminus C2$ for a general graph. If for a given image graph $G = (\mathcal{I}, \mathcal{A})$ and set of seeds $\mathcal{S}$, there exists an optimum-path forest for f, then any spanning forest P computed in G by Algorithm 1 for f is an optimum-path forest.*

Proof: Although, in the general case, the connectivity function f violates C2, for this particular graph, f actually satisfies the condition C2. Note that, for all $t \in \mathcal{I}$ we can take an optimum path $\pi_t = \pi_s \cdot \langle s,t \rangle$ where π_s is optimum from the existing optimum-path forest. Hence, f behaves as a smooth function for this particular graph, leading to optimum results. ■

When, on previous works, it is said that Algorithm 1 computes a spanning forest that may not be optimum for non-smooth functions, you might think that there was such an optimum-path forest, but the algorithm was not able to find it. However, as a consequence of Proposition 1, we have that for any connectivity function $f \in (C1 \cap C4) \setminus C2$, Algorithm 1 only fails to find an optimum-path forest, if no such forest exists. Thus, it is not a fault of the algorithm itself, but a fault of the problem specification which has no valid solution in the form of an optimum-path forest.

Proposition 2. *Consider a function $f \in (C1 \cap C4) \setminus C2$. For a given image graph $G = (\mathcal{I}, \mathcal{A})$, and set of seeds $\mathcal{S}$, let $\mathcal{O}$ be the set of all pixels $t \in \mathcal{I}$, such that there exists a complete-optimum path π_t for f. In any spanning forest P computed in G by Algorithm 1 for f, all the paths τ_t^P with $t \in \mathcal{O}$ are optimum paths.*

Proof: Let $\pi_t = \langle t_1, t_2, \ldots, t_i, \ldots, t_n = t \rangle$ be a given complete-optimum path for f, and $\tau_t^P = \langle s_1, s_2, \ldots, s_m = t \rangle$ be the computed path in the spanning forest P. We have the following proof by mathematical induction:

- **The basis:** Show that the statement holds for $n = 1$. In this case, we have $t = t_1$, and therefore $\pi_t = \langle t_1 \rangle$. Since $f(\langle t_1 \rangle)$ is a finite value, t_1 is inserted into the priority queue Q (Line 6 of Alg. 1). Since $f(\langle t_1 \rangle)$ is optimum, we can safely assure that it won't leave Q (Line 8) with a cost $V(t_1)$ worse than $f(\langle t_1 \rangle)$, therefore, the computed path τ_t^P must be optimum.
- **The inductive step:** Assume that the statement is true for the complete-optimum path π_{t_i}, $i \geq 1$. We must prove that it also holds for the complete-optimum path $\pi_{t_{i+1}} = \pi_{t_i} \cdot \langle t_i, t_{i+1} \rangle$. By the hypothesis we have that the path $\tau_{t_i}^P$ in P is optimum. Given that the condition C4 is satisfied ($f \in (C1 \cap C4) \setminus C2$), we may conclude that $f(\tau_{t_i}^P \cdot \langle t_i, t_{i+1} \rangle) = f(\pi_{t_i} \cdot \langle t_i, t_{i+1} \rangle) = f(\pi_{t_{i+1}})$, so we may conclude that $\tau_{t_i}^P \cdot \langle t_i, t_{i+1} \rangle$ is optimum. By algorithm construction, if t_{i+1} was not yet conquered, we have that this extended path $\tau_{t_i}^P \cdot \langle t_i, t_{i+1} \rangle$ will be evaluated by the Algorithm 1 (Lines 10-15), and since it is optimum, it won't be posteriorly replaced by any other path (as guaranteed by the strict inequality in Line 12). If t_{i+1} was already conquered by following a different path in P, its cost cannot be worse than $f(\pi_{t_{i+1}})$, because $f \in C1$. So in the end, $\tau_{t_{i+1}}^P$ will be an optimum path.

[3]The proof of their positions in the diagram were omitted due to the lack of space.

The successive application of the previous proposition gives a characterization of Algorithm 1 for $f \in (C1 \cap C4) \setminus C2$, as the result of a sequence of optimizations, where each optimization step involves a maximal set of elements, in a well-structured way.

Consider the following definitions: Let $\mathcal{E}^{set}(X) = \{\forall (s,t) \in \mathcal{A} \mid s \in X \wedge t \in X\}$ denote the set of all arcs interconnecting nodes in the set X, $\mathcal{E}^{path}(\pi)$ denote the set of all arcs in the path π (i.e., $\mathcal{E}^{path}(\pi) = \{\forall (t_i, t_{i+1})$ for $1 \leq i \leq k-1 | \ \pi = \langle t_1, t_2, \ldots, t_i, t_{i+1}, \ldots, t_k \rangle\}$), $\mathcal{E}^{cut}(X,Y) = \{\forall (s,t) \in \mathcal{A} | s \in X \wedge t \in Y\}$, $\mathcal{E}^{pred}(X) = \bigcup_{\forall t \in X} \mathcal{E}^{path}(\pi_t^P)$.

In the first optimization step, optimum paths τ_t^P are computed for all $t \in \mathcal{O}$ (Proposition 2). Let's denote $\mathcal{O}$ as $\mathcal{O}^1$ for this first step. In the next optimization step, consider the subgraph $G^2 = (\mathcal{I}, \mathcal{E}^{set}(\mathcal{I} \setminus \mathcal{O}^1) \cup \mathcal{E}^{cut}(\mathcal{O}^1, \mathcal{I} \setminus \mathcal{O}^1) \cup \mathcal{E}^{pred}(\mathcal{O}^1))$. A second path optimization is performed, by computing a second IFT, but now in G^2 [4]. Since the arcs interconnecting nodes in $\mathcal{O}^1$, are reduced to the arcs in the previous forest P (i.e., $\mathcal{E}^{pred}(\mathcal{O}^1)$) in G^2, we have that the optimum paths τ_t^P, computed on the previous step, will remain optimum in the new graph G^2. So the optimum paths τ_t^P with $t \in \mathcal{O}^1$ will start a new competition, seeking for their best extensions to the other pixels in $\mathcal{I} \setminus \mathcal{O}^1$. By applying the Proposition 2 on this new optimization problem one more time, we have that this second IFT will conquer a new maximal set of pixels $\mathcal{O}^1 \cup \mathcal{O}^2$ that can be reached by optimum paths in G^2. We can then repeat this process over again. The condition $C1$[5] guarantees that at least one new element will be conquered at each step, so that this process will repeat until $\bigcup_{\forall i} \mathcal{O}^i = \mathcal{I}$.

IV. Experiments

In this section, we present the quantitative analysis of the accuracy for segmenting the brain in 3D, in experiments involving a 3 Tesla MR-image dataset, containing ten T1-weighted 3D images. The image dataset included the head and, at least, a small portion of the neck of male and female adults with normal brains. A specialist delineated the ground-truths (GT)s. The seeds were chosen by a robot user, the method introduced by Gulshan et al. [19], to simulate user interaction of interactive segmentation by placing brush strokes automatically to iteratively, and interactively, complete the segmentation task. The procedure, including the choice of seeds (based on the knowledge of the ground truth) and the successive delineations, is iterative. The initial seeds for the object are placed at the point(s) in the object farthest from the boundary; similarly, for the background. At each successive iteration, the robot always places a spherical brush stroke in the largest connected component of the segmentation error area (placed at the point(s) farthest from the boundary of the component), and updates the segmentation. The process is repeated up to 25 times, generating a sequence of 25 simulated user strokes.

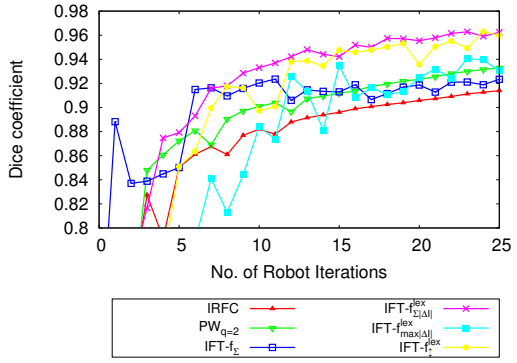

Fig. 2. Results using a robot user for segmenting the brain dataset.

We used a spherical brush with a diameter of 10 voxels. Figure 2 shows the experimental curves, where $IRFC$ and $PW_{q=2}$ represent different algorithms related to the smooth function $f_{\max}$ [17], [20], and we used $w(s,t) = G(s) + G(t)$, where $G(s)$ is the magnitude of Sobel gradient at a voxel s. Clearly, $f^{lex}_{\sum|\Delta I|}$ presented the best accuracy. Figure 3 shows one example for user-selected markers. These results emphasize the importance of non-smooth connectivity functions. The non-smooth connectivity function $f^{lex}_{\sum|\Delta I|}$ is a variation of $f_{\sum|\Delta I|}$ (Equation 9), in order to guarantee that $f^{lex}_{\sum|\Delta I|} \in (C1 \cap C4) \setminus C2$. This transformation is similar to the one used to get $f^{lex}_{\Sigma\max} \in (C1 \cap C4) \setminus C2$ from $f_{\Sigma\max}$ (see Appendix section). The function $f^{lex}_{\sum|\Delta I|}$ gives pairs of values that should be compared according to the lexicographical order. The first component is the non-smooth function $f_{\sum|\Delta I|}$ (Equation 9), and the second is the priority level of the seed/root for that path. The lower its value the higher is its priority. In interactive segmentation, we give lower priority for new inserted seeds, since they are used mainly for corrective actions, so that we can keep their effects more locally. The same process was done for $f^{lex}_{max|\Delta I|} \in (C1 \cap C4) \setminus C2$ and $f^{lex}_{\updownarrow} \in (C1 \cap C4) \setminus C2$, in relation to $f_{max|\Delta I|}$ (Eq. 8) and $f_{\updownarrow}$ (Eq. 5), respectively.

Although the results obtained by the smooth function $f_{\max}$ (e.g., $IRFC$) could be improved by using a better gradient-like image, this would require an undesirable training step (implicitly or explicitly) in order to enhance the object boundary [22]. IFT using $f^{lex}_{\sum|\Delta I|}$ not only avoids any training stage, but it can also better handle the inhomogeneity effects (Figure 4).

V. Conclusion

We have shown a promising subset of non-smooth connectivity functions (i.e., $f \in (C1 \cap C4) \setminus C2$), including a theoretical analysis of its properties. In particular, the function $f^{lex}_{\sum|\Delta I|}$ demonstrated very good results for the 3D segmentation of MR images of 3 Tesla. We intend to combine it with statistical models for automatic segmentation, and to extend this analysis to other non-smooth connectivity functions.

[4] By Algorithm 1, the pixels $s \in \mathcal{O}^1$ have $status(s) = 1$, and their paths can't be changed. Therefore, we consider a new graph G^2, where the edges interconnecting nodes in $\mathcal{O}^1$ which are not in the forest P are disregarded.

[5] By the hypothesis, we know that f satisfies the condition $C1$.

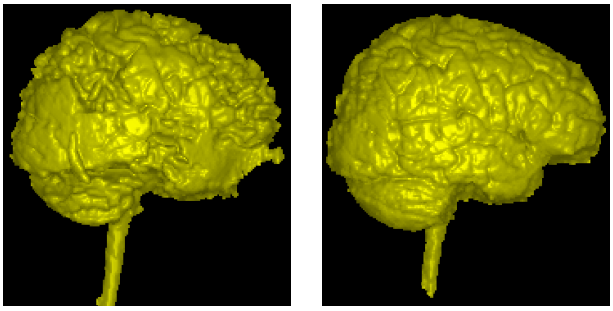

(a) (b)

Fig. 3. Brain segmentation results for the same user-selected markers by (a) $f_{\max}$, and (b) $f^{lex}_{\sum|\triangle I|}$.

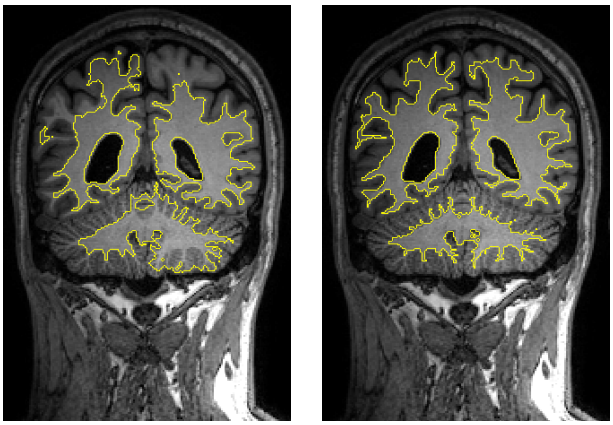

(a) (b)

Fig. 4. White matter segmentation in 3D for the same user-selected markers. Results by (a) $f_{\max}$ over an enhanced gradient, and (b) $f^{lex}_{\sum|\triangle I|}$.

ACKNOWLEDGMENT

The authors thank FAPESP (2012/06911-2), and CNPq (305381/2012-1) for the financial support.

REFERENCES

[1] P. Suetens, *Fundamentals of Medical Imaging*. Cambridge University Press, 2009.

[2] M. Sonka, R. Boyle, and V. Hlavac, *Image Processing, Analysis and Machine Vision*. ITP, 1999.

[3] A. Madabhushi and J. Udupa, "Interplay between intensity standardization and inhomogeneity correction in MR image processing," *IEEE Transactions on Medical Imaging*, vol. 24, no. 5, pp. 561–576, 2005.

[4] A. Falcão, J. Stolfi, and R. Lotufo, "The image foresting transform: Theory, algorithms, and applications," *IEEE Transactions on Pattern Analysis and Machine Intelligence*, vol. 26, no. 1, pp. 19–29, 2004.

[5] A. Falcão, F. Bergo, F. Favretto, G. Ruppert, P. Miranda, and F. Cappabianco, *Neurociências e epilepsia. Capítulo: Processamento, Visualização e Análise de Imagens Anatômicas do Cérebro Humano*. Plêiade, 2008, vol. 1, série CInAPCe.

[6] A. Falcão and F. Bergo, "Interactive volume segmentation with differential image foresting transforms," *IEEE Trans. on Medical Imaging*, vol. 23, no. 9, pp. 1100–1108, 2004.

[7] P. Miranda, A. Falcão, and J. Udupa, "Cloud bank: A multiple clouds model and its use in MR brain image segmentation," in *Proc. of the IEEE Intl. Symp. on Biomedical Imaging*, Boston, MA, 2009, pp. 506–509.

[8] F. Cappabianco, P. Miranda, J. Ide, C. Yasuda, and A. Falcão, "Unraveling the compromise between skull stripping and inhomogeneity correction in 3T MR images," in *SIBGRAPI 2012 (Conference on Graphics, Patterns and Images)*, Aug 2012, pp. 1–8.

[9] A. Falcão, L. Costa, and B. da Cunha, "Multiscale skeletons by image foresting transform and its applications to neuromorphometry," *Pattern Recognition*, vol. 35, no. 7, pp. 1571–1582, Apr 2002.

[10] R. Torres, A. Falcão, and L. Costa, "A graph-based approach for multiscale shape analysis," *Pattern Recognition*, vol. 37, no. 6, pp. 1163–1174, 2004.

[11] G. Herman and B. Carvalho, "Multiseeded segmentation using fuzzy connectedness," *IEEE Transactions on Pattern Analysis and Machine Intelligence*, vol. 23, pp. 460–474, May 2001.

[12] P. Miranda, A. Falcão, A. Rocha, and F. Bergo, "Object delineation by κ-connected components," *EURASIP Journal on Advances in Signal Processing*, pp. 1–14, 2008.

[13] R. Strand, K. Ciesielski, F. Malmberg, and P. Saha, "The minimum barrier distance," *Computer Vision and Image Understanding*, vol. 117, pp. 429–437, 2013.

[14] P. Miranda and L. Mansilla, "Oriented image foresting transform segmentation by seed competition," *IEEE Transactions on Image Processing*, 2013, accepted, to appear.

[15] L. Mansilla and P. Miranda, "Image segmentation by oriented image foresting transform: Handling ties and colored images," in *18th International Conference on Digital Signal Processing (DSP)*, Santorini, Greece, Jul 2013, accepted, to appear.

[16] P. Miranda, A. Falcão, and T. Spina, "Riverbed: A novel user-steered image segmentation method based on optimum boundary tracking," *IEEE Transactions on Image Processing*, vol. 21, no. 6, pp. 3042–3052, Jun 2012.

[17] K. Ciesielski, J. Udupa, P. Saha, and Y. Zhuge, "Iterative relative fuzzy connectedness for multiple objects with multiple seeds," *Computer Vision and Image Understanding*, vol. 107, no. 3, pp. 160–182, 2007.

[18] P. Saha and J. Udupa, "Relative fuzzy connectedness among multiple objects: Theory, algorithms, and applications in image segmentation," *Comp. Vision and Image Understanding*, vol. 82, no. 1, pp. 42–56, 2001.

[19] V. Gulshan, C. Rother, A. Criminisi, A. Blake, and A. Zisserman, "Geodesic star convexity for interactive image segmentation," in *Proc. of Computer Vision and Pattern Recognition*, 2010, pp. 3129–3136.

[20] C.Couprie, L.Grady, L.Najman, and H.Talbot, "Power watersheds: A unifying graph-based optimization framework," *Trans. on Pattern Anal. and Machine Intelligence*, vol. 99, 2010.

[21] P. Miranda and A. Falcão, "Links between image segmentation based on optimum-path forest and minimum cut in graph," *Journal of Mathematical Imaging and Vision*, vol. 35, no. 2, pp. 128–142, 2009.

[22] P. Miranda, A. Falcão, and J. Udupa, "Synergistic arc-weight estimation for interactive image segmentation using graphs," *Computer Vision and Image Understanding*, vol. 114, no. 1, pp. 85–99, Jan 2010.

APPENDIX A

A. Function $f_{\Sigma\max}$ (sum of $f_{\max}$)

Let $f_{\Sigma\max}$ be the function defined by:

$$\begin{aligned} f_{\Sigma\max}(\pi_t = \langle t\rangle) &= \begin{cases} 0, & \text{if } t \in S, \\ +\infty, & \text{otherwise.} \end{cases} \\ f_{\Sigma\max}(\pi_t = \pi_s \cdot \langle s,t\rangle) &= f_{\Sigma\max}(\pi_s) + f_{\max}(\pi_t), \quad (4) \end{aligned}$$

where S is a set of seeds.

From the diagram, we have that $f_{\Sigma\max} \in C1 \setminus (C2 \cup C4)$.

Proof:

C1. There is an optimum path $\pi_t = \pi_s \cdot \langle s,t\rangle$, such that $f_{\Sigma\max}(\pi_s) \leq f_{\Sigma\max}(\pi_t)$.
For $\omega(s,t) \geq 0$ we have that $f_{\max}(\pi_t) = \max\{f_{\max}(\pi_s), \omega(s,t)\} \geq 0$, then $f_{\Sigma\max}(\pi_s) \leq f_{\Sigma\max}(\pi_s) + f_{\max}(\pi_t)$. So, from (4) we obtain $f_{\Sigma\max}(\pi_s) \leq f_{\Sigma\max}(\pi_t)$. Therefore, $f_{\Sigma\max}$ satisfies this condition.

C2. There is an optimum path $\pi_t = \pi_s \cdot \langle s,t\rangle$, where π_s is optimum.

The proof that $f_{\Sigma\max}$ does not lie in C2 can be demonstrated by the following counterexample. In Fig. 5, for the optimum path $\pi_t = \pi_s \cdot \langle s,t\rangle$, we have that π_s is not an optimum path to s. There is another path π'_s that offers a better cost to s than π_s (i.e.$f_{\Sigma\max}(\pi'_s) = 9 \leq f_{\Sigma\max}(\pi_s) = 10$). So the condition C2 may not be verified for $f_{\Sigma\max}$.

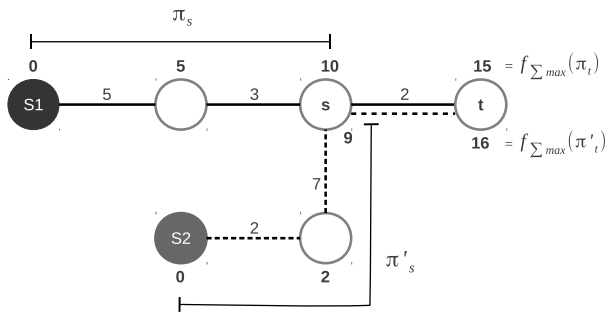

Fig. 5. Counterexample of the second and third conditions (C2 and C3) for the function $f_{\Sigma\max}$, where $\pi_t = \pi_s \cdot \langle s,t\rangle$ is an optimum path, and $\pi'_t = \pi'_s \cdot \langle s,t\rangle$ is a non-optimal path, from seeds s_1 and s_2, respectively.

C3. For any optimum path π'_s ending at s, $f_{\Sigma\max}(\pi'_s \cdot \langle s,t\rangle) = f_{\Sigma\max}(\pi_t)$.
In Fig. 5 we can observe that $f_{\Sigma\max}(\pi'_s \cdot \langle s,t\rangle) = 16 \neq f_{\Sigma\max}(\pi_t) = 15$. Hence, C3 is violated by $f_{\Sigma\max}$.

C4. For any paths π_s and π'_s ending at s, if $f_{\Sigma\max}(\pi_s) = f_{\Sigma\max}(\pi'_s)$, then we have $f_{\Sigma\max}(\pi_s \cdot \langle s,t\rangle) = f_{\Sigma\max}(\pi'_s \cdot \langle s,t\rangle)$.
In Fig. 6, for the optimum paths π_s and π'_s we have $f_{\Sigma\max}(\pi_s \cdot \langle s,t\rangle) = 15 \neq f_{\Sigma\max}(\pi'_s \cdot \langle s,t\rangle) = 16$.
Therefore, clearly we have that $f_{\Sigma\max}$ doesn't satisfy property C4.

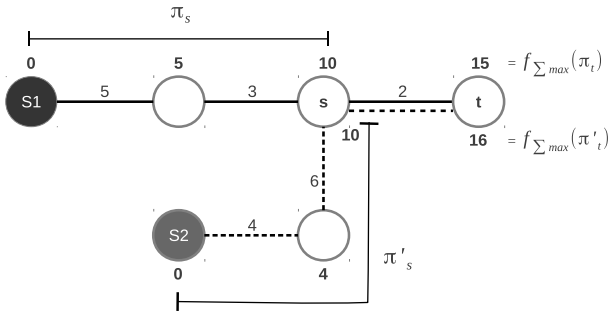

Fig. 6. Counterexample of the property C4 for the function $f_{\Sigma\max}$, where $\pi_t = \pi_s \cdot \langle s,t\rangle$, π_s, and π'_s are optimum paths, $\pi'_t = \pi'_s \cdot \langle s,t\rangle$ is a non-optimal path, and s_1, s_2 are seeds.

B. The barrier distance function

Let $f_{\updownarrow}$ be the function defined by:

$$\begin{aligned} f_{\updownarrow}(\pi_t = \langle t\rangle) &= \begin{cases} 0, & \text{if } t \in S, \\ +\infty, & \text{otherwise.} \end{cases} \\ f_{\updownarrow}(\pi_t = \pi_s \cdot \langle s,t\rangle) &= f_{Imax}(\pi_t) - f_{Imin}(\pi_t), \end{aligned} \quad (5)$$

where S is a set of seeds, and f_{Imax} and f_{Imin} are functions that take the maximum and minimum intensity values along the path, respectively:

$$\begin{aligned} f_{Imax}(\pi_t = \langle t\rangle) &= I(t) \\ f_{Imax}(\pi_t = \pi_s \cdot \langle s,t\rangle) &= max\{f_{Imax}(\pi_s), I(t)\}, \end{aligned} \quad (6)$$

and

$$\begin{aligned} f_{Imin}(\pi_t = \langle t\rangle) &= I(t) \\ f_{Imin}(\pi_t = \pi_s \cdot \langle s,t\rangle) &= min\{f_{Imin}(\pi_s), I(t)\}, \end{aligned} \quad (7)$$

where $I(t)$ is the intensity of a pixel t.

From the diagram, we have that $f_{\updownarrow} \in C1 \setminus (C2 \cup C4)$.

Proof:

C1. $f_{\updownarrow}(\pi_s) \leq f_{\updownarrow}(\pi_t)$.
Since $f_{Imax}(\pi_s) \leq f_{Imax}(\pi_t)$, and $f_{Imin}(\pi_t) \leq f_{Imin}(\pi_s)$, then, $f_{Imax}(\pi_s) + f_{Imin}(\pi_t) \leq f_{Imax}(\pi_t) + f_{Imin}(\pi_s)$ and, $f_{Imax}(\pi_s) - f_{Imin}(\pi_s) \leq f_{Imax}(\pi_t) - f_{Imin}(\pi_t)$. So, from (5) we obtain $f_{\updownarrow}(\pi_s) \leq f_{\updownarrow}(\pi_t)$. Hence, $f_{\updownarrow}$ satisfies the condition C1.

C2. π_s is optimum.
In Fig. 7, for the optimum path $\pi_t = \pi_s \cdot \langle s,t\rangle$, we have that π_s is not optimum, since there is another path π'_s which offers a better cost than π_s to s (i.e., $f_{\updownarrow}(\pi'_s) = 6 \leq f_{\updownarrow}(\pi_s) = 7$). Hence, C2 does not hold for $f_{\updownarrow}$.

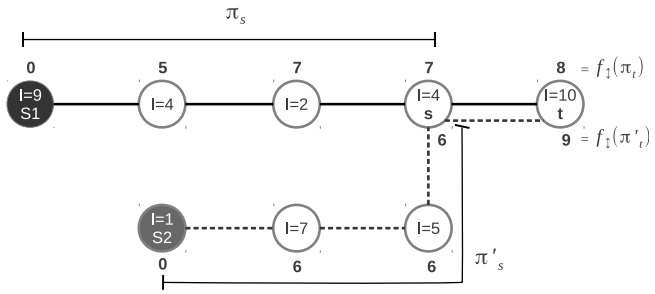

Fig. 7. Counterexample for the second and third conditions (C2 and C3) for the function $f_{\updownarrow}$, where $\pi_t = \pi_s \cdot \langle s,t\rangle$ is an optimum path, and $\pi'_t = \pi'_s \cdot \langle s,t\rangle$ is a non-optimal path, from seeds s_1 and s_2, respectively.

C3. For any optimum path π'_s, $f_{\updownarrow}(\pi'_s \cdot \langle s,t\rangle) = f_{\updownarrow}(\pi_t)$.
In Fig. 7 we have $f_{\updownarrow}(\pi'_s \cdot \langle s,t\rangle) = 9 \neq f_{\updownarrow}(\pi_t = \pi_s \cdot \langle s,t\rangle) = 8$. Hence, we have that $f_{\updownarrow} \notin C3$.

C4. For any paths π_s and π'_s ending at s, if $f_{\updownarrow}(\pi_s) = f_{\updownarrow}(\pi'_s)$, then $f_{\updownarrow}(\pi_s \cdot \langle s,t\rangle) = f_{\updownarrow}(\pi'_s \cdot \langle s,t\rangle)$. In Fig. 8, for the optimum paths π_s and π'_s we have:
$f_{\updownarrow}(\pi_s \cdot \langle s,t\rangle) = 5 \neq f_{\updownarrow}(\pi'_s \cdot \langle s,t\rangle) = 7$.
Consequently, $f_{\updownarrow}$ doesn't satisfy this property ($f_{\updownarrow} \notin C4$).

C. Peak amplitude of the relative intensity ($f_{max|\triangle I|}$)

Let $f_{max|\triangle I|}$ be the function defined by:

$$\begin{aligned} f_{max|\triangle I|}(\pi_t = \langle t\rangle) &= \begin{cases} 0, & \text{if } t \in S, \\ +\infty, & \text{otherwise.} \end{cases} \\ f_{max|\triangle I|}(\pi_t = \pi_s \cdot \langle s,t\rangle) &= max\{f_{max|\triangle I|}(\pi_s), \\ &\qquad |I(t) - I(R(\pi_s))|\}, \end{aligned} \quad (8)$$

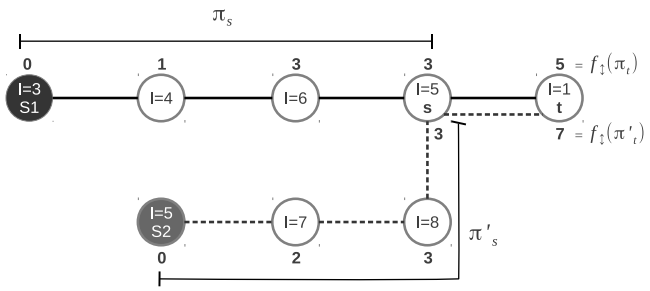

Fig. 8. Counterexample of the property C4 for the function $f_{\updownarrow}$, where $\pi_t = \pi_s \cdot \langle s,t \rangle$, π_s, and π'_s are optimum paths, $\pi'_t = \pi'_s \cdot \langle s,t \rangle$ is a non-optimal path, and s_1, s_2 are seeds.

where $R(\pi_s)$ is the root pixel (origin) of the path π_s.

From the diagram, we have that $f_{max|\triangle I|} \in C1 \backslash (C2 \cup C4)$.

Proof:

C1. $f_{max|\triangle I|}(\pi_s) \leq f_{max|\triangle I|}(\pi_t)$.
Suppose that this condition is true, then from (8) we have: $f_{max|\triangle I|}(\pi_s) \leq max\{f_{max|\triangle I|}(\pi_s), |I(t) - I(R(\pi_s))|\}$, which is clearly right, because of the max function on the second term. Hence, $f_{max|\triangle I|}(\pi_s)$ satisfies C1.

C2. π_s is optimum.
In Fig. 9, for the optimum path $\pi_t = \pi_s \cdot \langle s,t \rangle$, we have that π_s is not optimum, since there is another path π'_s which offers a better cost than π_s to s (i.e., $f_{max|\triangle I|}(\pi'_s) = 7 \leq f_{max|\triangle I|}(\pi_s) = 8$). So, $f_{max|\triangle I|}$ violates the condition C2 ($f_{max|\triangle I|} \notin C2$).

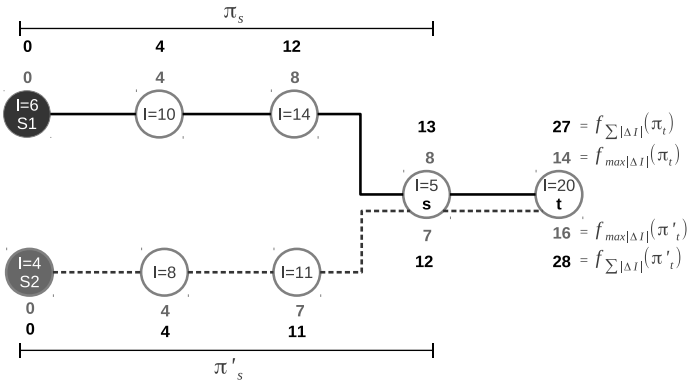

Fig. 9. Counterexamples of the second and third conditions (C2 and C3) for the functions $f_{max|\triangle I|}$ and $f_{\Sigma|\triangle I|}$. The path $\pi_t = \pi_s \cdot \langle s,t \rangle$ is an optimum path, and $\pi'_t = \pi'_s \cdot \langle s,t \rangle$ is a non-optimal path, from seeds s_1 and s_2, respectively.

C3. For any optimum path π'_s, $f_{max|\triangle I|}(\pi'_s \cdot \langle s,t \rangle) = f_{max|\triangle I|}(\pi_t)$
We can see a counterexample in Fig. 9, where this condition is violated (i.e., $f_{max|\triangle I|}(\pi'_s \cdot \langle s,t \rangle) = 16 \neq f_{max|\triangle I|}(\pi_t) = 14$).

C4. For any paths π_s and π'_s ending at s, if $f_{max|\triangle I|}(\pi_s) = f_{max|\triangle I|}(\pi'_s)$, then $f_{max|\triangle I|}(\pi_s \cdot \langle s,t \rangle) = f_{max|\triangle I|}(\pi'_s \cdot \langle s,t \rangle)$.
In Fig. 10, we can observe that: $f_{max|\triangle I|}(\pi_s \cdot \langle s,t \rangle) = 14 \neq f_{max|\triangle I|}(\pi'_s \cdot \langle s,t \rangle) = 16$. Hence, $f_{max|\triangle I|}$ doesn't satisfy this property ($f_{max|\triangle I|} \notin C4$).

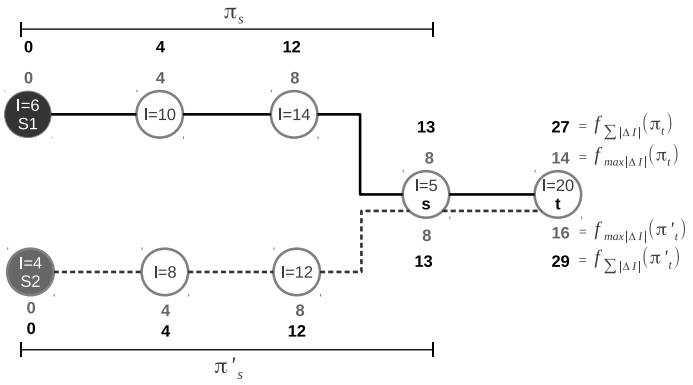

Fig. 10. Counterexamples of the condition C4 for the functions $f_{max|\triangle I|}$ and $f_{\Sigma|\triangle I|}$. The paths $\pi_t = \pi_s \cdot \langle s,t \rangle$, π_s, and π'_s are optimum, $\pi'_t = \pi'_s \cdot \langle s,t \rangle$ is a non-optimal path, and s_1, and s_2 are seeds.

D. Sum of the absolute value of relative intensities

Let $f_{\sum|\triangle I|}$ be the function defined by:

$$\begin{aligned} f_{\sum|\triangle I|}(\pi_t = \langle t \rangle) &= \begin{cases} 0, & \text{if } t \in S, \\ +\infty, & \text{otherwise.} \end{cases} \\ f_{\sum|\triangle I|}(\pi_t = \pi_s \cdot \langle s,t \rangle) &= f_{\sum|\triangle I|}(\pi_s) + |I(t) - I(R(\pi_s))|, \end{aligned} \tag{9}$$

where $R(\pi_s)$ is the root pixel (origin) of the path π_s.

Proof:

C1. $f_{\Sigma|\triangle I|}(\pi_s) \leq f_{\Sigma|\triangle I|}(\pi_t)$.
Suppose that this condition is true, then from (9) we have: $f_{\Sigma|\triangle I|}(\pi_s) \leq f_{\Sigma|\triangle I|}(\pi_s) + |I(t) - I(R(\pi_s))|$
As $|I(t) - I(R(\pi_s))| \geq 0$ this relation is right, so the condition C1 is satisfied ($f_{\Sigma|\triangle I|} \in C1$).

C2. π_s is optimum.
In Fig. 9, for the optimum path $\pi_t = \pi_s \cdot \langle s,t \rangle$, we have that π_s is not optimum, since there is another path π'_s that has a better cost than π_s (i.e., $f_{\Sigma|\triangle I|}(\pi'_s) = 12 \leq f_{\Sigma|\triangle I|}(\pi_s) = 13$). So, this condition is not satisfied ($f_{\Sigma|\triangle I|} \notin C2$).

C3. For any optimum path π'_s, $f_{\Sigma|\triangle I|}(\pi'_s \cdot \langle s,t \rangle) = f_{\Sigma|\triangle I|}(\pi_t)$
The counterexample in Fig. 9 shows that this condition is violated (i.e., $f_{\Sigma|\triangle I|}(\pi'_s \cdot \langle s,t \rangle) = 28 \neq f_{\Sigma|\triangle I|}(\pi_t) = 27$).

C4. For any paths π_s and π'_s ending at s, if $f_{\Sigma|\triangle I|}(\pi_s) = f_{\Sigma|\triangle I|}(\pi'_s)$, then $f_{\Sigma|\triangle I|}(\pi_s \cdot \langle s,t \rangle) = f_{\Sigma|\triangle I|}(\pi'_s \cdot \langle s,t \rangle)$.
In Fig. 10, for the optimum paths π_s and π'_s we have: $f_{\Sigma|\triangle I|}(\pi_s \cdot \langle s,t \rangle) = 27 \neq f_{\Sigma|\triangle I|}(\pi'_s \cdot \langle s,t \rangle) = 29$.
Hence, $f_{\Sigma|\triangle I|}$ doesn't satisfy this property.

E. Function of intensity

Let f_I be the function defined by:

$$\begin{aligned} f_I(\pi_t = \langle t \rangle) &= \begin{cases} 0, & \text{if } t \in S, \\ +\infty, & \text{otherwise.} \end{cases} \\ f_I(\pi_t = \pi_s \cdot \langle s,t \rangle) &= I(t), \end{aligned} \tag{10}$$

where S is a set of seeds.

Proof:

C1. $f_I(\pi_s) \leq f_I(\pi_t)$.
In Fig. 11 we have $f_I(\pi_s) = 30 \not\leq f_I(\pi_t) = 20$. So, this condition is violated.

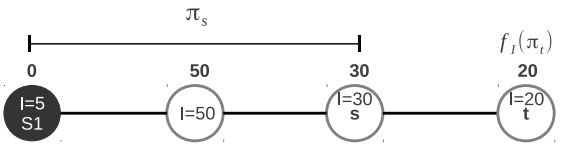

Fig. 11. Counterexample of the first condition (C1) for the function f_I, where $\pi_t = \pi_s \cdot \langle s, t\rangle$ is an optimum path, and $s1$ is a seed.

C2. π_s is optimum.
This can be proved by contradiction as follows:
For $\pi_t = \pi_s \cdot \langle s, t\rangle$ optimum, if π_s is not optimum then it is true that there exists an optimum path π'_s, such that $f_I(\pi'_s) = I(s) < f_I(\pi_s) = I(s)$, which is false, leading to a contradiction. Therefore, C2 is satisfied by f_I.

C3. For any optimum path π'_s ending at s, $f_I(\pi'_s \cdot \langle s, t\rangle) = f_I(\pi_t)$.
This condition is also satisfied, since $f_I(\pi'_s \cdot \langle s, t\rangle) = I(t)$ and $f_I(\pi_t) = I(t)$.

C4. For any paths π_s and π'_s ending at s, if $f_I(\pi_s) = f_I(\pi'_s)$, then $f_I(\pi_s \cdot \langle s, t\rangle) = f_I(\pi'_s \cdot \langle s, t\rangle)$.
This property is satisfied, because for any π_s, $f_I(\pi_s \cdot \langle s, t\rangle) = I(t)$.

Thus, function f_I violates condition C1, and is not smooth.

F. Function lexicographic sum of $f_{\max}$

Let $f^{lex}_{\Sigma\max}$ be the function defined by:

$$f^{lex}_{\Sigma\max}(\pi_t = \langle t\rangle) = \begin{cases} (0,0), & \text{if } t \in S, \\ (+\infty, +\infty), & \text{otherwise.} \end{cases}$$

$$f^{lex}_{\Sigma\max}(\pi_t = \pi_s \cdot \langle s, t\rangle) = (f_{\Sigma\max}(\pi_t), f_{\max}(\pi_t)). \quad (11)$$

where S is a set of seeds.
This function $f^{lex}_{\Sigma\max}$ gives pairs of values that should be compared according to the lexicographical order. The first component is the non-smooth function $f_{\Sigma\max}$, and the second is the smooth function $f_{\max}$.

Proof:

C1. $f^{lex}_{\Sigma\max}(\pi_s) \leq f^{lex}_{\Sigma\max}(\pi_t)$.
Suppose that this is true. Then, from (11) we have:

$$(f_{\Sigma\max}(\pi_s), f_{\max}(\pi_s)) \leq (f_{\Sigma\max}(\pi_t), f_{\max}(\pi_t)). \quad (12)$$

By comparing the ordered pairs we obtain:

$$f_{\Sigma\max}(\pi_s) < f_{\Sigma\max}(\pi_t), \quad (13)$$

or

$$f_{\Sigma\max}(\pi_s) = f_{\Sigma\max}(\pi_t) \text{ and } f_{\max}(\pi_s) \leq f_{\max}(\pi_t) \quad (14)$$

Since both $f_{\Sigma\max}$ and $f_{\max}$ satisfy condition C1 for $w(s,t) \geq 0$ (see Section V-A), we may conclude that $f^{lex}_{\Sigma\max} \in C1$ for $w(s,t) \geq 0$.

C2. π_s is optimum.
In Fig. 12, for the optimum path $\pi_t = \pi_s \cdot \langle s, t\rangle$, we have that π_s is not optimum, since there is another path π'_s that offers a better cost than π_s (i.e., $f^{lex}_{\Sigma\max}(\pi'_s) = (9,7) \leq f^{lex}_{\Sigma\max}(\pi_s) = (10,5)$). Therefore, this condition is not satisfied by $f^{lex}_{\Sigma\max}$.

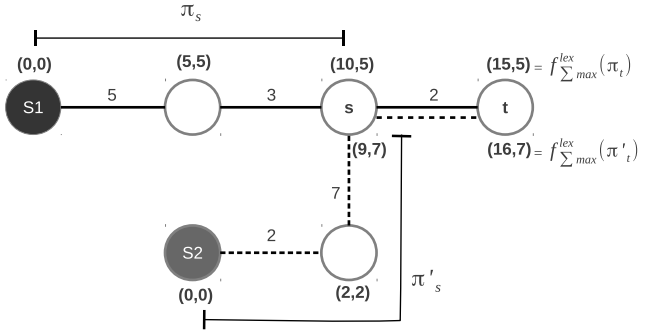

Fig. 12. Counterexample of the second and third conditions (C2 and C3) for the function $f^{lex}_{\Sigma\max}$, where $\pi_t = \pi_s \cdot \langle s, t\rangle$ is an optimum path, and $\pi'_t = \pi'_s \cdot \langle s, t\rangle$ is a non-optimal path, from the seeds s_1 and s_2, respectively.

C3. For any optimum path π'_s, $f^{lex}_{\Sigma\max}(\pi'_s \cdot \langle s, t\rangle) = f^{lex}_{\Sigma\max}(\pi_t)$
In Fig. 12 we have
$f^{lex}_{\Sigma\max}(\pi'_s \cdot \langle s, t\rangle) = (16,7) \neq f^{lex}_{\Sigma\max}(\pi_t) = (15,5)$.
Hence, this condition is violated by $f^{lex}_{\Sigma\max}$.

C4. For any paths π_s and π'_s ending at s, if $f^{lex}_{\Sigma\max}(\pi_s) = f^{lex}_{\Sigma\max}(\pi'_s)$, then $f^{lex}_{\Sigma\max}(\pi_s \cdot \langle s, t\rangle) = f^{lex}_{\Sigma\max}(\pi'_s \cdot \langle s, t\rangle)$.
Given that $f^{lex}_{\Sigma\max}(\pi_s) = f^{lex}_{\Sigma\max}(\pi'_s)$, from (11) we obtain $(f_{\Sigma\max}(\pi_s), f_{\max}(\pi_s)) = (f_{\Sigma\max}(\pi'_s), f_{\max}(\pi'_s))$, which implies that:

$$f_{\Sigma\max}(\pi_s) = f_{\Sigma\max}(\pi'_s), \text{ and} \quad (15)$$
$$f_{\max}(\pi_s) = f_{\max}(\pi'_s). \quad (16)$$

Hence, by the definition of $f_{\max}$ and from (16)

$$f_{\max}(\pi_s \cdot \langle s, t\rangle) = \max\{f_{\max}(\pi'_s),\ \omega(s,t)\},$$
$$f_{\max}(\pi_s \cdot \langle s, t\rangle) = f_{\max}(\pi'_s \cdot \langle s, t\rangle) \quad (17)$$

and from (4), (15), and (17) we have

$$f_{\Sigma\max}(\pi_s \cdot \langle s, t\rangle) = f_{\Sigma\max}(\pi'_s) + f_{\max}(\pi'_s \cdot \langle s, t\rangle),$$
$$f_{\Sigma\max}(\pi_s \cdot \langle s, t\rangle) = f_{\Sigma\max}(\pi'_s \cdot \langle s, t\rangle) \quad (18)$$

So, from (17) and (18) we have

$$f^{lex}_{\Sigma\max}(\pi_s \cdot \langle s, t\rangle) = (f_{\Sigma\max}(\pi'_s \cdot \langle s, t\rangle), f_{\max}(\pi'_s \cdot \langle s, t\rangle)),$$
$$f^{lex}_{\Sigma\max}(\pi_s \cdot \langle s, t\rangle) = f^{lex}_{\Sigma\max}(\pi'_s \cdot \langle s, t\rangle) \quad (19)$$

Therefore, the property C4 is satisfied by $f^{lex}_{\Sigma\max}$.

Thus, we have that the function $f^{lex}_{\Sigma\max}$ is a non-smooth function that violates only the conditions C2 and C3. Note that $f^{lex}_{\Sigma\max}$ does not violate C4, as opposed to $f_{\Sigma\max}$.